11th International Symposium on Magnetic Bearings
August 26-29, Nara, Japan

LQR CONTROL OF A BEARINGLESS MACHINE IMPLEMENTED WITH A DSP

Wilmar L. Kauss
LASUP – Dept. of Electrical Engg., UFRJ, Rio de Janeiro RJ 21941-972 Brasil
wilmarlk@hotmail.com

A. C. Del Nero Gomes
Electrical Engg. Program, COPPE –UFRJ, Rio de Janeiro RJ 21941-972 Brasil
afel@coep.ufrj.br

Richard M. Stephan *
LASUP – Dept. of Electrical Engg., UFRJ, Rio de Janeiro RJ 21941-972 Brasil
richard@coe.ufrj.br

Domingos F. B. David
PGMEC, UFF – Universidade Federal Fluminense, Niterói RJ 21941-972 Brasil
domingos@vm.uff.br

ABSTRACT
Magnetic devices are used as bearings in important practical applications like high speeds, high vacuum, low temperatures, clean and explosive atmospheres. In conventional magnetic bearings the restoring forces are generated by electromagnets; in bearingless motors a single element is used for spinning and positioning the rotor. One way of achieving this hybrid solution is by rearranging the windings of an electrical motor in such a way as to provide both torque and radial restoring forces.

The hardware of those devices comprises an electromechanical part, sensors, power electronic amplifiers and microelectronic circuits for the control. Any performance improvement achieved by changing the control software adds practically no cost to the overall budget. The effort to develop and implement better control algorithms is, therefore, justified.

A prototype of a vertical rotor is currently in development at COPPE/UFRJ. In its actual stage the rotor vertical position is kept by a mechanical bearing and it is driven and horizontally stabilized by a bearingless motor. Aspects of the modelling procedures for the device are reported in this paper, as well as results of an optimal control strategy based on the centralized and decentralized Linear Quadratic Regulator and its digital implementation.

*LASUP acknowledges the financial support received from CNPq and FAPERJ

INTRODUCTION
Magnetic Bearings and Bearingless Machines are mechatronic systems with growing technological applications in fields like high speeds, high vacuum, low temperatures, clean and explosive atmospheres [1], [2]. The study of magnetic bearings has reached a mature stage, as can be seen from the vast amount of publications, a brief list of which is: [3], [4], [5], and the previously cited ones.

A more sophisticated version of magnetic bearings has been studied in the last decade: instead of using distinct elements for spinning and positioning the rotor, a hybrid solution was devised where multiple functions are executed by a single **Bearingless Motor**. The literature for this field is not so vast: [1], [5], [6], [7], [8], [9], [10], [11].

There are three ways to generate the bearingless effect. One uses Lorentz forces, ([7], [12]) and the remaining rely on Maxwell forces, obtained through additional windings, [1], or by splitting the wind-

ings of a conventional machine ([10], [13]). A split winding configuration will be studied in this paper: the windings of an induction motor are rearranged in such a way as to simultaneously provide torque and radial positioning forces. Figure 1 shows a vertical rotor driven and stabilized by a bearingless motor, which is currently in development at COPPE/UFRJ: [5], [10], [11], [14], [15], [16].

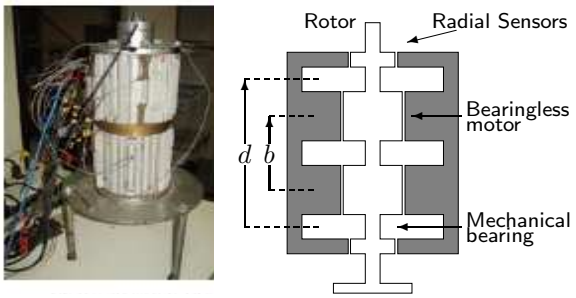

Figure 1: Prototype views — $d = .31$m, $b = .23$m

The hardware of such a device comprises an electromechanical part, sensors, power electronic amplifiers and microelectronic circuits for the control. Any performance improvement that can be achieved with the same hardware, by just changing the control software, adds practically no cost to a series production. Therefore, the effort to implement better control algorithms is justified. This paper presents experimental results of a bearingless machine controlled with a Linear Quadratic Regulator (LQR). The laboratory prototype , the mathematical model, the establishment of coupled and decoupled feedback control laws will be explained. The experimental results will be discussed.

In the next section a brief description of the system will be given, together with some modeling details of the motor-bearings; after that, the dynamic aspects of the full system are modeled, and then the complete mathematical model of the system, together with the control strategy results obtained with LQ control laws is presented. Some details about the implementation, the overall performance and the conclusions are given in the final sections.

DESCRIPTION

The sensors at the upper part of the prototype measure displacements in orthogonal directions. The clearance between the sensor heads and the targets in the rotor is 0.4mm; security roller bearings are displayed just above the sensor targets with a smaller radial gap of 0.3mm. The rotor is passively supported by the mechanical bearing shown in the lower position.

The bearingless motor can be considered as a 4-pole 2-phase induction machine. A sketch of its stator is seen in figure 2;

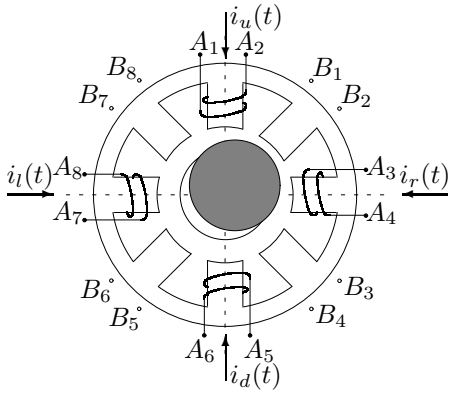

Figure 2: Diagram of the 4-pole 2-phase stator

When the four coils of each phase are connected in series (A_2 to A_3, etc) and the phases are fed with currents with the same amplitude and a 90° phase difference the device generates torque. When the amplitudes of the currents in the poles of phase A are independently controlled, but their angles are the same, and still 90° different from those of phase B, the device is able to spin the shaft and to keep it at the central position. In phase B: $i_B(t) = I_0 \cos \omega t$; the "poles" of phase A are fed with independent (base and differential) currents: $i_A(t) = I_0 \sin \omega t$, $i_x(t) = u_x \sin \omega t$ and $i_y(t) = u_y \sin \omega t$:

$$i_l(t) = i_A(t) - i_x(t) \qquad i_r(t) = i_A(t) + i_x(t) \quad (1)$$

$$i_u(t) = i_A(t) - i_y(t) \qquad i_d(t) = i_A(t) + i_y(t) \quad (2)$$

When a radial displacement is detected, the control system modifies the amplitudes u_x and u_y to correct it. The current amplitudes should be kept within sufficiently low level in order to avoid saturation of the motor magnetic circuit. The radial forces generated by the motor-bearing are

$$f_x = 2k_p x + k_i[1 - \cos(2\omega t)]u_x \quad (3)$$

$$f_y = 2k_p y + k_i[1 - \cos(2\omega t)]u_y \quad (4)$$

where x and y are the rotor displacements. It should be stressed that k_p and k_i are not constants, as the formulas above suggest, they depend on the rotor electrical frequency $\sigma\omega$: $k_p = k_p(\sigma\omega), k_i = k_i(\sigma\omega)$. If $\cos(2\omega t)$ could be neglected, a simpler expression would be attained: $f_x = k_p x + k_i u_x$. But k_p and k_i still depend on the operating conditions. Detailed explanations can be found in [9].

SYSTEM DYNAMICS

Figure 3 shows the standard ([2], [4]) reference system placed at the mechanical bearing, which is assumed to be a perfect articulation. The center of mass (CM) position is determined by the angles α and β. The rotor moments of inertia with respect to the axes x and y are the same, because of symmetry: $J = J_x = J_y$; the moment of inertia with respect to z is I_z. Newton's rotational dynamic laws are:

$$J\ddot{\beta} - \omega_r I_z \dot{\alpha} = \sum p_y; \quad J\ddot{\alpha} + \omega_r I_z \dot{\beta} = \sum p_x \quad (5)$$

where ω_r is the angular velocity and p_y, p_x represent the external torques on the device. The gravity action (simulations show) can be neglected, leaving only the torques due to the bearingless motor:

$$p_x = -f_y b \cos\alpha \quad \text{and} \quad p_y = f_x b \cos\beta \quad (6)$$

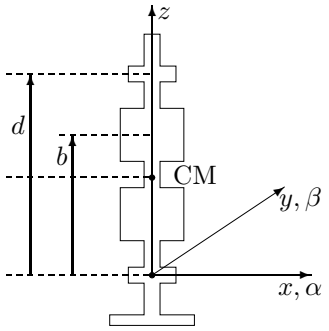

Figure 3: The rotor and the reference system

The bearingless forces come from (3) and (4); with x_b and y_b denoting the rotor displacement at position b:

$$\begin{bmatrix} f_x \\ f_y \end{bmatrix} = 2k_p \begin{bmatrix} x_b \\ y_b \end{bmatrix} + k_i(1 - \cos 2\omega t) \begin{bmatrix} u_x \\ u_y \end{bmatrix} \quad (7)$$

Since $\cos\alpha \approx \cos\beta \approx 1$, because the angles are very small, (6) and (7) become

$$\begin{bmatrix} p_y \\ -p_x \end{bmatrix} = K_p \begin{bmatrix} x_b \\ y_b \end{bmatrix} + K_u \begin{bmatrix} u_x \\ u_y \end{bmatrix} \quad (8)$$

where $K_p = 2bk_p$ and $K_u = bk_i(1 - \cos 2\omega t)$. Assuming again small angles lead to $x_b = b\beta$ and $y_b = -b\alpha$; these equations, with (8), are used to rewrite (5) in vector form

$$J\ddot{\theta} + \omega_r I_z \begin{bmatrix} 0 & 1 \\ -1 & 0 \end{bmatrix} \dot{\theta} = bK_p\theta + K_u \begin{bmatrix} u_x \\ u_y \end{bmatrix} \quad (9)$$

where $\theta = [\beta \quad -\alpha]^T$ and the first order term coefficient, the gyroscopic matrix, will be denoted by G. In order to display the dynamic equation in terms of the displacements measured by the sensors notice that, because of small angles, $\sin\beta \approx \beta = x_d/d$ and $\sin\alpha \approx \alpha = -y_d/d$ which amounts to $\theta = d^{-1} z_d$ where $z_d = [\ x_d \quad y_d\ ]^T$. The result, where $u = [u_x \ \ u_y]^T$ is the control vector, is

$$\ddot{z_d} + GJ^{-1}\dot{z_d} - bK_pJ^{-1}z_d = dK_uJ^{-1}u \quad (10)$$

CONTROLLING THE POSITION

Defining the state vector $x = [\,x_d \ \ y_d \ \ \dot{x}_d \ \ \dot{y}_d\,]^T$ it is possible to transform (10) into the canonical form

$$\dot{x}(t) = Ax(t) + \Gamma(t)u(t) \quad (11)$$

where A and $\Gamma(t)$ are (4×4) and (4×2) matrices given by

$$A = \begin{bmatrix} 0 & I_2 \\ A_{21} & A_{22} \end{bmatrix} \text{ and } \Gamma(t) = \begin{bmatrix} 0 \\ \Gamma_2(t) \end{bmatrix} \quad (12)$$

Block I_2 is the (2×2) identity matrix and

$$A_{21} = bdK_pJ^{-1}I_2 \qquad A_{22} = -GJ^{-1}$$

$$\Gamma_2(t) = dK_uJ^{-1}I_2$$

It should be noticed that both K_p and K_u depend, like k_p and k_i did, on the rotor electrical frequency $\sigma\omega$: $K_p = K_p(\sigma\omega), K_i = K_i(\sigma\omega)$; K_u depends also on t and the gyroscopic matrix G depends on the rotor velocity ω_r. This means that A_{21} and A_{22} are constant matrices only in steady-state conditions. The definition of K_u leads to

$$\Gamma_2(t) = dbk_iJ^{-1}(1 - \cos 2\omega t)I_2$$

and a linear model for the steady-state functioning of the positioning system is:

$$\dot{x}(t) = Ax(t) + Bu(t) - Bu(t)\cos 2\omega t \quad (13)$$

where the input matrix B is given by

$$B = \begin{bmatrix} 0 \\ B_2 \end{bmatrix} \quad \text{with} \quad B_2 = dbk_i J^{-1} \begin{bmatrix} 1 & 0 \\ 0 & 1 \end{bmatrix}$$

This is a linear time invariant (LTI) model, with a slowly varying control input $u(t)$ that also acts, after modulation by $\cos 2\omega t$, as a disturbance signal. A block diagram is seen in figure 4.

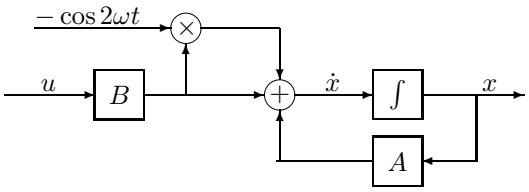

Figure 4: LTI model for the positioning system

If one wants to use the reluctance forces in AC motors cores for positioning purposes, the price to pay is the high frequency disturbance signal. It is reasonable to expect that the overall system contains enough mechanical inertias to make it behave as a low-pass filter. In this case the frequencies in $\cos 2\omega t$ would be "absorbed by the mass" and a simpler model would result. Several simulations were made showing that this is indeed the case, and the model described in equation (13) can be replaced by the traditional

$$\dot{x}(t) = Ax(t) + Bu(t) \tag{14}$$

Many of the available control schemes require models like (14). If an optimal control option is made, based on the Linear Quadratic Regulator (LQR), the solution will be

$$u(t) = F^* x(t) \tag{15}$$

Using well known procedures (for example, [4]) F^* is found after choosing weighting matrices Q and R and solving an Algebraic Riccati Equation. With this strategy F^* turns out to be a (2×4) full matrix, where few, or almost none, of its elements are zero, and this results in a great computational effort placed on the control algorithms. It would, therefore, be nice to impose a sparser structure to F^*, like the following:

$$F_d^* = \begin{bmatrix} p_1 & 0 & d_1 & 0 \\ 0 & p_2 & 0 & d_2 \end{bmatrix} \tag{16}$$

Such a matrix allows a decentralized control structure in which the two input variables are treated in an independent and uncoupled way, each one of them depending on just two state variables, a position and its derivative ([2]). This is called an optimal, decentralized, PD control. The traditional LQR theory has been adapted to this decentralized restriction. In what may be called the LQRd problem, there is a search for a decentralized structure, as above, that is capable of minimizing the same performance index used for the centralized case. More information in [4], [5] and [9].

EXPERIMENTAL RESULTS

Figures 5 to 8 below depict the rotor operation at 1500rpm. Figure 5 shows the effects of a decoupled LQRd control law and figure 6 shows the operation with a standard PD controller, as reported in [17]. In both graphs the horizontal scale is 50ms/div and the vertical scale is 0.05mm/div.

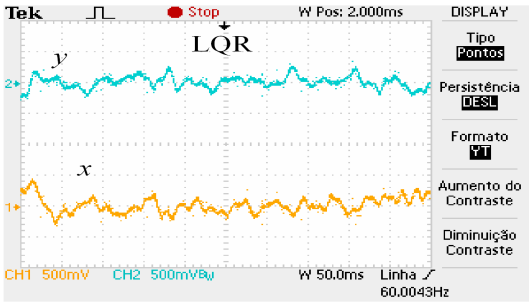

Figure 5: Measured time response with LQRd

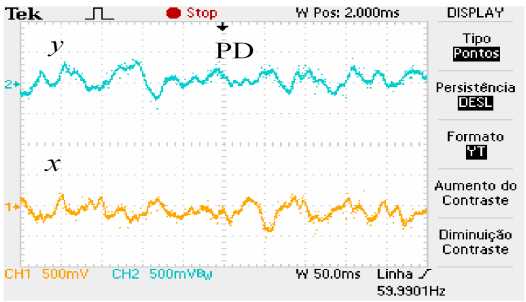

Figure 6: Measured time response with PD control

These results can be complemented with the correspondent Lissajous graphs shown in figures 7

and 8, obtained from screen shots with 5s persistence. For these graphs the scale in both axes is 0.1mm/div, and the outer circular borders represent the maximal rotor displacements.

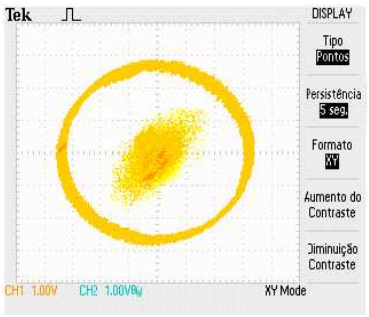

Figure 7: Measured xy response with LQRd

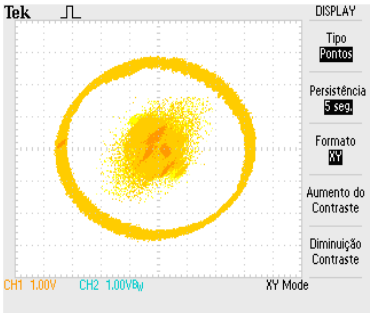

Figure 8: Measured xy response with PD control

The sampling frequency used was 32.8KHz (sampling period 30.5μs). The computational times of these algorithms can be seen and compared in Table 1, which also shows the results for the LQR, the centralized case. With a small computational time, the LQRd algorithm introduces a higher control flexibility and a better overall performance.

Table 1: Computational times in μs

Controller type	Sampling period		usage
	processing	idle	%
PD	20.4	9.9	66.9
LQRd	19.8	10.7	64.9
LQR	26.4	3.7	87.9

Figures 9 and 10 exhibit a time scale zoom of the controller input and output (I/O) signals. There are 100 samples in the horizontal axis; since the sampling time is 30.5μs, this leads to an observation window with width of approximately 3.05ms. The output signals, seen in the upper part of the graphs, is the incremental current value Δi; the input signals shown in the lower portions of the graphs is the position error.

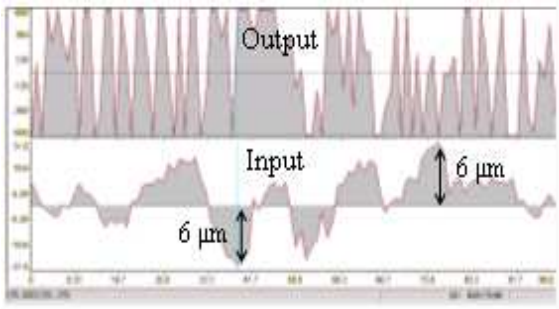

Figure 9: LQRd controller I/O signals at 1500rpm

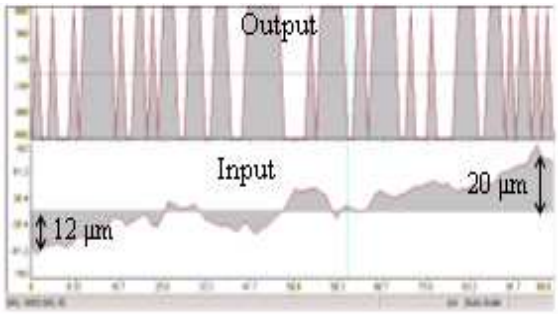

Figure 10: PD controller I/O signals at 1500rpm

CONCLUSIONS

Both controllers maintain the rotor position within small deviations from the central position, but the LQRd maximal error is lower than half (25% in some cases) the maximal values of the PD algorithm.

In conclusion, the LQRd controller has a better performance in terms of computational time and positioning, besides a straightforward design procedure. The main advantage of PD or PID controllers is the availability of standard algorithms. Due to the particular decentralized scheme used here, the

LQRd can be viewed as a PD controller with optimally chosen parameters.

References

[1] A. Chiba, T. Fukao, O. Ichikawa, M. Oshima, M. Takemoto, and D. Dorrell, *Magnetic Bearings and Bearingless Drives*. Elsevier, 2005.

[2] G. Schweitzer, H. Bleuler, and A. Traxler, *Active Magnetic Bearings*. Vdf Hochschulverlag AG an der ETH Zürich, 1994.

[3] C. R. Knospe and E. G. Collins, "Introduction to the special issue on magnetic bearing control," *IEEE Tansactions on Control Systems Technology*, vol. 4, no. 5, pp. 481–483, september 1996.

[4] H. Bleuler, "Decentralized control of magnetic rotor bearing systems," Doctor of Technical Sciences dissertation, Swiss Federal Institute of Technology, Zürich, 1984.

[5] D. F. B. David, A. C. D. N. Gomes, J. A. Santisteban, A. Ripper, R. de Andrade Jr., and R. Nicolsky, "A hybrid levitating rotor with radial electromagnetic motor-bearings and axial sc bearing," in *Proceedings of the MAGLEV 2000*, Rio, June 2000, pp. 441–446.

[6] A. Chiba, T. Deido, T. Fukao, and M. A. Rahman, "An analysis of bearingless ac motors," *IEEE Tansactions on Energy Conversion*, vol. 9, no. 1, pp. 61–68, 1994.

[7] R. Schob and J. Bichsel, "Vector control of the bearingless motor," *ISMB*, pp. 61–68, 1994.

[8] A. O. Salazar, A. Chiba, and T. Fukao, "A review of developments in bearingless motors," in *Proceedings of the Seventh International Symposium on Magnetic Bearings*, Zürich, August 2000, pp. 335 –.

[9] D. F. B. David, "Levitação de rotor por mancais-motores radiais magnéticos e mancal axial sc auto-estável," D. Sc. tese, COPPE–UFRJ, 2000.

[10] A. O. Salazar and R. M. Stephan, "A bearingless method for induction machines," *IEEE Trans. on Magnetism*, vol. 29, pp. 2965–2967, November 1993.

[11] J. A. Santisteban, D. F. B. David, R. Noronha, A. Ripper, and R. M. Stephan, "Controller design for a bearingless electric motor," in *Proc. of DYNAME—7th Intl. Conf. on Dynamic Problems in Mechanics*, March 1997, pp. 169–171.

[12] J. Bichsel, "The bearingless electrical machine," *NASA Conference Publication*, vol. 3152, no. 2, pp. 561–573, 1991.

[13] W. K. S. Khoo, R. L. Fittro, and S. D. Garvey, "Ac polyphase self-bearing motors with a bridge configured winding," in *Proc. of the 11th Intl. Symp. on Magnetic Bearings*, August 2002, pp. 47–52.

[14] R. Nicolsky, Y. Gorelov, A. S. Pereira, D. F. B. David, J. A. Santisteban, R. M. Stephan, A. Ripper, R. de Andrade Jr., W. Gawalek, T. Habisreuther, and T. Strasser, "Superconducting axial bearing for induction machines with active radial magnetic bearings," *IEEE Trans. on Applied Superconductivity*, vol. 9, pp. 964–967, 1999.

[15] R. Nicolsky, R. de Andrade Jr., A. Ripper, D. F. B. David, J. A. Santisteban, R. M. Stephan, W. Gawalek, T. Habisreuther, and T. Strasser, "Superconducting electromagnetic hybrid bearing using ybco bulk blocks for passive axial levitation," *Superconductor Science and Technology*, vol. 13, pp. 1–5, 2000.

[16] N. N. Cardoso, "Controle simultâneo de velocidade e posição em mancais motores magnéticos," M. Sc. tese, COPPE–UFRJ, 2003.

[17] R. R. Gomes, "Motor mancal com controle implementado em um dsp," M. Sc. tese, COPPE–UFRJ, 2007.